

## Nanostructure Design Using Protein Building Blocks Enhanced by Conformationally Constrained Synthetic Residues<sup>†</sup>

Jie Zheng,<sup>‡</sup> David Zanuy,<sup>§</sup> Nurit Haspel,<sup>||</sup> Chung-Jung Tsai,<sup>‡</sup> Carlos Alemán,<sup>§</sup> and Ruth Nussinov<sup>\*,‡,||</sup>

Basic Research Program, SAIC-Frederick, Inc., Center for Cancer Research Nanobiology Program, NCI-FCRDC, Frederick, Maryland 21702, Departament d'Enginyeria Química, E. T. S. d'Enginyeria Industrial de Barcelona, Universitat Politècnica de Catalunya, Diagonal 647, Barcelona E-08028, Spain, and Sackler Institute of Molecular Medicine, Department of Human Genetics and Molecular Medicine, Sackler School of Medicine, Tel Aviv University, Tel Aviv 69978, Israel

Received August 16, 2006; Revised Manuscript Received November 16, 2006

**ABSTRACT:** Increasing efforts are being invested in the construction of nanostructures with desired shapes and physical and chemical properties. Our strategy involves nanostructure design using naturally occurring protein building blocks. Inspection of the protein structural database (PDB) reveals the richness of the conformations, shapes, and chemistries of proteins and their building blocks. To increase the population of the native fold in the selected building block, we mutate natural residues by engineered, constrained residues that restrict the conformational freedom at the targeted site and have favorable interactions, geometry, and size. Here, as a model system, we construct nanotubes using building blocks from left-handed  $\beta$ -helices which are commonly occurring repeat protein architectures. We pick two-turn  $\beta$ -helical segments, duplicate and stack them, and using all-atom molecular dynamics simulations (MD) with explicit solvent probe the structural stability of these nanotubular structures as indicated by their capacity to retain the initial organization and their conformational dynamics. Comparison of the results for the wild-type and mutated sequences shows that the introduction of the conformationally restricted 1-aminocyclopropanecarboxylic acid (Ac<sub>3</sub>C) residue in loop regions greatly enhances the stability of  $\beta$ -helix nanotubes. The Ac<sub>3</sub>C geometrical confinement effect is sequence-specific and position-specific. The achievement of high stability of nanotubular structures originates not only from the reduction of mobility at the mutation site induced by Ac<sub>3</sub>C but also from stabilizing association forces between building blocks such as hydrogen bonds and hydrophobic contacts. For the selected synthetic residue, similar size, hydrophobicity, and backbone conformational tendencies are desirable as in the Ac<sub>3</sub>C.

The design of self-assembled nanostructures has important potential biomedical applications such as antiviral drug carriers, scaffolds for tissue repair, and spectroscopic labels for therapeutic and photonic applications (1–3). The considerable efforts which have been invested have achieved remarkable progress toward obtaining supramolecules consisting of self-assembled synthetic polymers (4). However, successful design of synthetic polymers for biomedical applications remains a challenge due to their biocompatibility, biological activity and specificity, solubility, and degradability (5). Only a few therapeutic studies exist in vivo under physiological conditions (6). Yet, detailed structural, functional, and morphological information is available for numerous peptides and proteins (7), and self-assembly of

those proteins/peptides into well-defined 2D and 3D nanostructures is a common process in many natural systems. Peptides and proteins are known to form ordered amyloid fibrils with a predominance of secondary structures consisting of  $\beta$ -strands. Surfactant-like peptides form nanotubes (8, 9) and nanowires (10, 11). The type 1 human immunodeficiency virus (HIV-1) capsid protein (CA) subunits can spontaneously assemble into complex tubular/conical/spherical viral structures in vitro (12, 13). However, a complete understanding of the kinetic process of the self-assembly into complex nanostructures and the nanostructure–function relationship in the living cell is still lacking.

Our approach for already a number of years involves protein and nanostructure design using naturally occurring protein building blocks. Construction of stable nanostructures with different shapes using natural building blocks appears to be a reasonable strategy toward precisely and quantitatively controlling the supramolecular assemblies. A building block is a structural unit which, if cut from the protein chain and placed in solution, is still likely to have a conformation similar to the one it has when embedded in the native protein structure (14). That is, its preferred conformational state is the native state. The Protein Data Bank is populated by an extensive repertoire of building blocks, with different shapes,

<sup>†</sup> This project has been funded in whole or in part by Federal funds from the National Cancer Institute, National Institutes of Health, under contract number NO1-CO-12400. This research was supported (in part) by the Intramural Research Program of the NIH, National Cancer Institute, Center for Cancer Research.

\* Address correspondence to this author at the Center for Cancer Research Nanobiology Program, NCI-Frederick, Building 469, Room 151, Frederick, MD 21702. E-mail: ruthn@ncifcrf.gov. Fax: 301-846-5598. Phone: 301-846-5579.

<sup>‡</sup> NCI-FCRDC.

<sup>§</sup> Universitat Politècnica de Catalunya.

<sup>||</sup> Tel Aviv University.

sizes, and chemical properties which can be used in design (15). Using building blocks has advantages, since these structural elements have been perfected by evolution, are easily available, and are biocompatible. The challenge is to be able to predictably modulate them toward the desired design goal. To successfully engineer nanostructures using naturally occurring building blocks, two criteria should be fulfilled. First, the selected building block should have a high population time in the desired conformation, and second, the association between the building blocks should be favorable, with an energy gap between the desired self-assembly and all other potential associations. To fulfill the first criterion, selection of a relatively stable structural unit such as a structural repeat taken from a commonly occurring repeat protein architecture (16–21) appears a promising choice. For the second, attempting to preserve a native interface or construct a closely related analogue also appears a reasonable approach (22). Nevertheless, naturally occurring systems are perfected by evolution toward a particular function. In general, protein function requires that the protein not be too stable since protein flexibility is often crucial. In contrast, for a designed nanostructure stability is likely to be the key. Thus, to enhance the population time of the building block, our group has been engineering conformationally restricted residues (23) which would be inserted or substituted for natural residues. The constrained motion limits the dynamics at the mutated site.

Experimentally, to predictably design, synthesize, manipulate, and fabricate novel nanostructures at the molecular level is still a highly challenging task. Due to recent advances in efficient simulation algorithms and high-performance computing, large-scale atomistic molecular dynamics simulations have provided valuable insights by exploring the molecular properties of structural models. Since simulations can quickly probe many models and provide potentially good candidate nanostructures in terms of structural stability and minimum free energy for experimental test, they could accelerate the design process.

*An Overview of Our System: Stacked  $\beta$ -Helical Conformational Motifs Enhanced by Synthetic Residues.*  $\beta$ -Helical proteins are promising candidates for designing nanostructures since (i) they contain highly repetitive, symmetrical building blocks (16) which could be used easily and readily to develop novel nanomaterials such as nanotubes and nanofibers without performing many structural manipulations and (ii) they mostly occur in or near active or binding sites, thus likely to be of functional importance. Many naturally occurring proteins (24–34) have been found to contain  $\beta$ -helical fragments that can fold into a helical, tubular or fibrillar architecture. As compared with right-handed  $\beta$ -helices, left-handed  $\beta$ -helices exhibit small variability of shape, size, and sequence. Typically, they have an equilateral triangular shape and highly repetitive sequence (35). In contrast, the sequences and shapes of right-handed  $\beta$ -helices are less regular. Guo et al. (36) presented a structural model for the A $\beta$  amyloid fibril core structure using a series of left-handed and right-handed  $\beta$ -helical proteins. They found that the core structure based on left-handed  $\beta$ -helical proteins was much more stable than the one based on right-handed  $\beta$ -helical proteins. By combining molecular modeling and electron crystallographic data, Govaerts and colleagues (26) reported that the structure of prions in the plastic region was

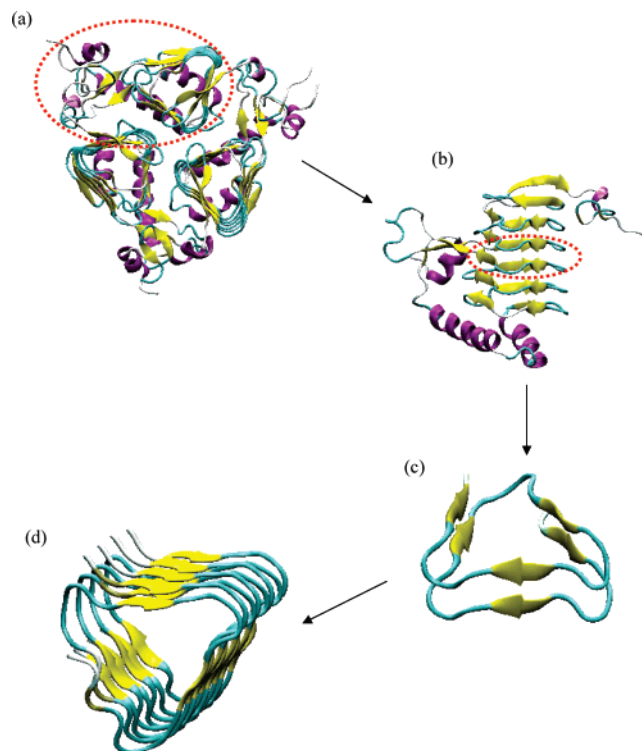


FIGURE 1: An illustration of the schematic procedure of the construction of a nanotube using the naturally occurring protein building block from a  $\beta$ -helix (taken from galactoside acetyltransferase, PDB code 1KRR). (a) The trimeric crystal structure of galactoside acetyltransferase (GAT) from *E. coli*, with three left-handed parallel  $\beta$ -helix domains. (b) The monomeric structure of GAT (circled) taken from the trimeric GAT structure. (c) A single building motif (circled) taken from the monomeric 1KRR structure with selected residues 131–165. (d) A nanotubular structure obtained by stacking four repetitive building motifs on top of each other.

compatible with a trimeric model, with left-handed, parallel  $\beta$ -helices. Thus, the left-handed  $\beta$ -helical building blocks are well suited for the design of nanostructures.

Here, we adopted a “bottom-up” approach to construct stable nanotubular structures from monomeric naturally occurring  $\beta$ -helical building blocks. We obtained  $\beta$ -helical motifs by slicing  $\beta$ -helices into two-turn repeat units. We computationally stacked four copies of the repeat unit on top of each other, with no covalent linkage between them (Figure 1), followed by the assessment of the feasibility of the construct, which was performed via relatively short all-atom simulations (37–43). Constructs which do not preserve their organization in the simulations are unlikely to preserve their organization in experiment; those that preserve their organization in the simulations are candidates for experiment. We selected repeats capable of tube organization and introduced conformationally restricted residues in strategic positions in order to reduce the conformational freedom and increase the relative weight of the desired repeat fold. The relative stabilities of the mutated proteins were probed by simulations.

Previously (15, 44), we examined nanostructures constructed from a broad range of potential motifs. Here, we focused on the most and least stable motifs. MD simulations were performed to test the structural stability and dynamics of the nanotubular structures constructed by the two left-handed  $\beta$ -helical peptides. To enhance the thermodynamic

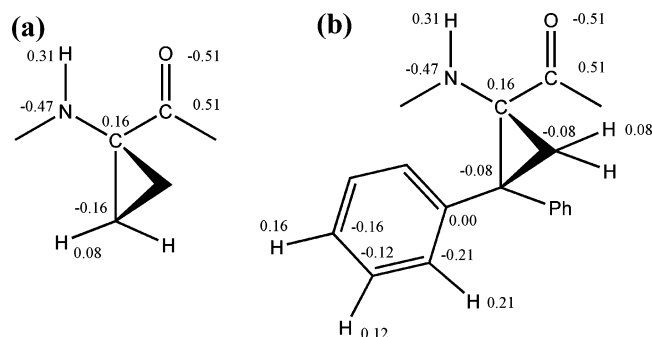


FIGURE 2: Schematic representation of (a)  $Ac_3c$  and (b)  $c_3Dip$  with labeled atomic charges.

stability of a given  $\beta$ -helical repeat sequence, we engineered chemically constrained residues with backbone conformational tendencies similar to those of natural amino acids in the most mobile (loop) regions. Among the synthetic residues that our group has prepared and studied, here we focused on 1-aminocyclopropanecarboxylic acid ( $Ac_3c$ ), a simple cyclic  $\alpha,\alpha$ -dialkylated amino acid with strong stereochemical constraints induced by the highly strained cyclopropane ring. We also tested its double-phenyl derivative, 1-amino-2,2-diphenylcyclopropanecarboxylic acid ( $c_3Dip$ ), a cyclopropane analogue of phenylalanine bearing two geminal phenyl rings. However, this substitution was unsuccessful, due to the steric effects induced by the residue side chain size.

**Survey of  $Ac_3c$  Derivatives.**  $Ac_3c$  is the simplest achiral  $C^\alpha$ -tetrasubstituted  $\alpha$ -amino acid with  $C^\alpha \leftrightarrow C^\alpha$  cyclization (Figure 2a). The stereochemical constraints of this amino acid are produced by the unfavorable steric interaction of the two  $\beta$ -methylene groups and by the three-membered ring rigidity. The conformational preferences of  $Ac_3c$  have been characterized by energy computations of the mono-peptide (45–47) and X-ray diffraction analyses (48–51) of a variety of peptides of this residue up to the tetramer level. These illustrated that the  $Ac_3c$  amino acid prefers the “bridge” region of the Ramachandran map, i.e.,  $(\varphi, \psi) \approx (\pm 80^\circ, 0^\circ)$ , which corresponds to position  $i + 2$  of type  $I/I'$  and type  $II/II'$   $\beta$ -turns.

Theoretical studies indicated that the tendency of  $Ac_3c$  to adopt a small value of  $\psi$  is due to the hyperconjugation between the lone pairs of the carbonyl oxygen of the residue and some adjacent molecular orbitals associated with the  $C^\beta-C^\beta$  bond (52). This conjugative ability of the  $Ac_3c$  cyclopropyl moiety was demonstrated by X-ray crystallography. The  $N-C^\alpha$  and  $C^\alpha-C$  bond lengths are significantly shortened compared to  $C^\alpha$ -trisubstituted and  $C^\alpha$ -tetrasubstituted  $\alpha$ -amino acids (53), and the mean exocyclic  $N-C^\alpha-C$  bond angle is significantly larger ( $116-118^\circ$ ) than the tetrahedral angle ( $109.5^\circ$ ). Thus, the strong tendency of  $Ac_3c$  to adopt  $\beta$ -turn conformations is enhanced by specific intraresidue electronic interactions.

Incorporation of selectively oriented side substituents into conformationally restricted amino acids allows increased control of the backbone fold (54). Cyclopropane analogues of phenylalanine are particularly attractive because the rigidly oriented phenyl side groups may interact with the backbone sterically and electronically through the aromatic  $\pi$ -orbitals (49, 51, 55). The side chain orientation of 1-amino-2-phenylcyclopropanecarboxylic acid ( $c_3Phe$ ) stereoisomers drastically affects the backbone conformational preferences,

with a tendency to adopt folded conformations (52, 56, 57). This tendency was observed in the stereoisomers of 1-amino-2,3-diphenylcyclopropanecarboxylic acid with the phenyl substituents in a *trans* relative disposition ( $c_3diPhe$ ) (55, 58) in both solid state and solution. A cyclopropane analogue of phenylalanine bearing two geminal phenyl side substituents was recently incorporated into Pro- $c_3Dip$ . X-ray diffraction analysis showed that the (*S*)-Pro-(*R*)- $c_3Dip$  stereoisomer adopts two consecutive  $\gamma$ -turns stabilized by intramolecular hydrogen bonds (59). The ability of  $c_3Dip$  to adopt a  $\gamma$ -turn and to induce this structural motif in neighboring amino acids was explained by calculations (60). The dihedral angle  $\psi$  values for all cyclopropane analogues of phenylalanine are close to  $0^\circ$  due to the presence of hyperconjugative effects (52, 58, 60). It is worth noting that interesting supramolecular structures have been characterized for peptides rich in  $c_3Dip$  (61, 62).

Here we focused on  $Ac_3c$ , the simplest  $C^\alpha$ -tetrasubstituted cyclic  $\alpha$ -amino acid promoting  $\beta$ -turn-type conformations, and  $c_3Dip$  (Figure 2b), in which the  $Ac_3c$  conformational preferences are guided toward the  $\gamma$ -turn. Force field parameters for  $Ac_3c$  and its derivatives were explicitly developed (Figure 2 and refs 45 and 46).

## METHODS

**Left-Handed  $\beta$ -Helical Peptides.** Two protein fragments (PDB codes 1KRR and 1HV9), derived from left-handed  $\beta$ -helical proteins, were selected to introduce a targeted replacement by the conformationally restricted  $Ac_3c$  residue in this work. The 1KRR (63) is obtained from galactoside acetyltransferase from *Escherichia coli* (residues 131–165) and the 1HV9 (64) from *N*-acetylglucosamine-1-phosphate uridylyltransferase GlnU, C-terminal domain from *E. coli* (residues 296–329). Both X-ray crystal structures of 1KRR and 1HV9 show that these two protein fragments have an almost perfect equilateral triangular shape, with each side being  $\sim 18$  Å. Each sequence contains a repetitive helical strand-loop motif, where the peptide backbones alternate between  $\beta$ -strands and loops. 1KRR exhibits three short loops at positions of Pro1, Pro18, Gly19 (loop 1), Ser12, Hsd13, Ala30, Gly31 (loop 2), and Asn6, Asn7, Asp24, Asn25 (loop 3), while 1HV9 exhibits three similar short loops at positions of Pro16, Tyr17, Pro33, Phe34 (loop 1), Lys4, Asn5, Glu21, Asp22 (loop 2), and Asp10, Asp11, Ala27, Ala28 (loop 3) (Figure 3). The interior protein core is mainly packed by hydrophobic side chains. The bulky hydrophobic residues (Ile and Val) predominantly stack in the center while smaller residues (Ala and Thr) are in the corner. To construct the candidate nanotubular structures, four repeated subunits are stacked on top of each other with an intermolecular distance between two neighboring subunits of 4.8 Å. The N-terminal is acetylated and the C-terminal is amidated to avoid terminal charges.

**MD Simulation Protocols.** All molecular dynamics simulations were conducted by using the NAMD program (65) with the all-atom CHARMM27 force field (66). Each system was solvated in a TIP3P water box with a minimum distance of at least 8 Å from any edge of the box to any protein atom. Any water molecule within 2.4 Å of the peptide was removed. We followed the standard protocol for each MD simulation, which consists of an initial minimization, heating

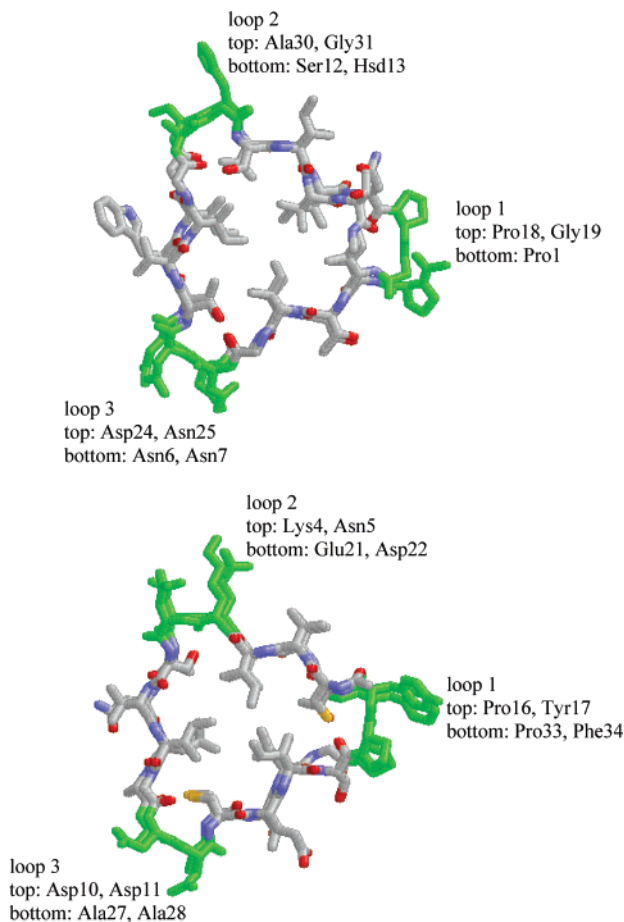


FIGURE 3: A stick representation of a top view of a single left-handed  $\beta$ -helical building block subunit of 1KRR (residues 131–165) (upper panel) and of 1HV9 (residues 296–329) (lower panel). Each building block is a two-turn unit (the two helical turns are marked as “top” and “bottom”). Residues in the loop regions are displayed as green sticks; residues in the  $\beta$ -sheet region are in gray. Hydrogen atoms are omitted for clarity.

procedure, equilibrium, and production run. Each system was initially energy minimized to remove unfavorable contacts using the conjugate gradient method for 3000 steps. The system was then subjected to 200 ps of heating procedure from 50 to 330 K with a position constraint imposed on the peptides to allow relaxation of water molecules. The following 500 ps equilibrium run was performed with position constraints on the protein. The production run was carried out in the NPT ensemble (1 atm and 330 K) using 3D periodic boundary conditions with the minimum image convention. The temperature was controlled at 330 K by a Langevin thermostat with a damping coefficient of  $5 \text{ ps}^{-1}$ , while the pressure was maintained at 1 bar by a Langevin piston with a decay period of 100 fs and a damping time of 50 fs. During the simulations, all covalent bonds involving hydrogen were constrained by using the SHAKE algorithm so that a time step was set to 2 fs. The short-range van der Waals (VDW) interactions were calculated by the switch function with a twin range cutoff of 10.0 and 12.0 Å, and the long-range electrostatic interactions were calculated by the force shift function with a cutoff of 12.0 Å. Nonbonded neighbor lists were updated automatically on the basis of the heuristic algorithm. Each system was simulated for 12 ns at 330 K, and the trajectories were saved at 1.0 ps intervals

Table 1: Summary of the Model Systems

Systems	Sequence	Mutation Position	Repeat Units (Simulation Times, ns)	
<b>1KRR</b>				
A1	PITIGNNVWIGSHVVIN PGVTIGD <del>N</del> SVIGAGSIVT	---	1 (4 ns)	4 (12 ns)
A2	PITIGNNVWIGSHVVIN PGVTIGD <del>N</del> SVIGAGSIVT	Ala30	1 (4 ns)	4 (12 ns)
A3	PITIG <del>N</del> VWIGSHVVIN PGVTIGD <del>N</del> SVIGAGSIVT	Asn7, Asn25	1 (4 ns)	4 (12 ns)
A4	PITIGNNVWIGSHVVIN PGVTIGD <del>N</del> SVIGAGSIVT	Ser12, Ala30	1 (4 ns)	4 (12 ns)
A5	PITIGNNVWIGSHVVIN PGVTIGD <del>N</del> SVIGAGSIVT	His13, Gly31	1 (4 ns)	4 (12 ns)
<b>1HV9</b>				
B1	CVIKNSVIGDDCEISPY TVVEDANLAAACTIGPF	---	1 (4 ns)	4 (12 ns)
B2	CVIKNSVIGDDCEISPY TVVEDANLAAACTIGPF	Ala26	1 (4 ns)	4 (8 ns)
B3	CVIKNSVIGDDCEISPY TVVEDANLAAACTIGPF	Ala27	1 (4 ns)	4 (12 ns)
B4	CVIKNSVIGDDCEISPY TVVEDANLAAACTIGPF	Asp10, Ala27	1 (4 ns)	4 (12 ns)
B5	CVIKNSVIGDDCEISPY TVVEDANLAAACTIGPF	Asp11, Ala28	1 (4 ns)	4 (12 ns)
B6	CVIKNSVIGDDCEISPY TVVEDANLAAACTIGPF	Asn5, Asn22	1 (4 ns)	4 (12 ns)
B7	CVIKNSVIGDDCEISPY TVVEDANLAAACTIGPF	Asn5, Ala27	1 (4 ns)	4 (12 ns)

for later analysis. A summary of the model systems is given in Table 1.

*Analysis Details.* The conformational stability of the nanostructure is measured by a calculation of the backbone root mean square deviation (RMSD) relative to the initial structure throughout the simulations.

The overall size of a given structure is measured by its radius of gyration ( $R_{\text{gyr}}$ ).  $R_{\text{gyr}}$  is defined as the mass-weighted geometric mean of the distance of each atom from the protein’s center of mass:

$$R_{\text{gyr}} = \sqrt{\frac{\sum_{i=1}^n m_i (r_i - r_{\text{com}})^2}{\sum_{i=1}^n m_i}}$$

The secondary structure is monitored by computing the backbone  $\varphi$ ,  $\psi$  dihedral angles at each loop region. The  $\varphi$ ,  $\psi$  angles cluster into distinct regions according to the following definitions (67):  $\alpha_L$  region,  $\psi = -30^\circ$  to  $100^\circ$ ;  $\varphi = 30^\circ$  to  $100^\circ$ ;  $\alpha_R$  region,  $\psi = -20^\circ$  to  $-60^\circ$ ;  $\varphi = -40^\circ$  to  $-90^\circ$ ;  $\beta$  region,  $\psi = 75^\circ$  to  $180^\circ$ ;  $\varphi = -100^\circ$  to  $180^\circ$ ; bridge region,  $\psi = -20^\circ$  to  $75^\circ$ ;  $\varphi = -40^\circ$  to  $180^\circ$ . A narrowly distributed  $\varphi$ ,  $\psi$  dihedral angle indicates that the side chains of the amino acid are constrained in their movements.

The native contacts consist of backbone hydrogen bonds and side chain contacts (40). A hydrogen bond is assigned if the distance between donor D and acceptor A is  $\leq 3.6$  Å and the angle D–H...A is  $\geq 120^\circ$ , and a side chain contact is defined if the distance between the center of mass of two adjacent side chains is less than 6.7 Å.

To examine the nanostructural integrity, the average mass center distance between adjacent building subunits is measured to characterize the peptide associations.

A hydrophobic contact is defined when the center of mass of distance between two hydrophobic side chains is less than 4 Å.

## RESULTS

To avoid redundant terminology, the notation used in this study to denote a mutant is indicated by the one letter residue

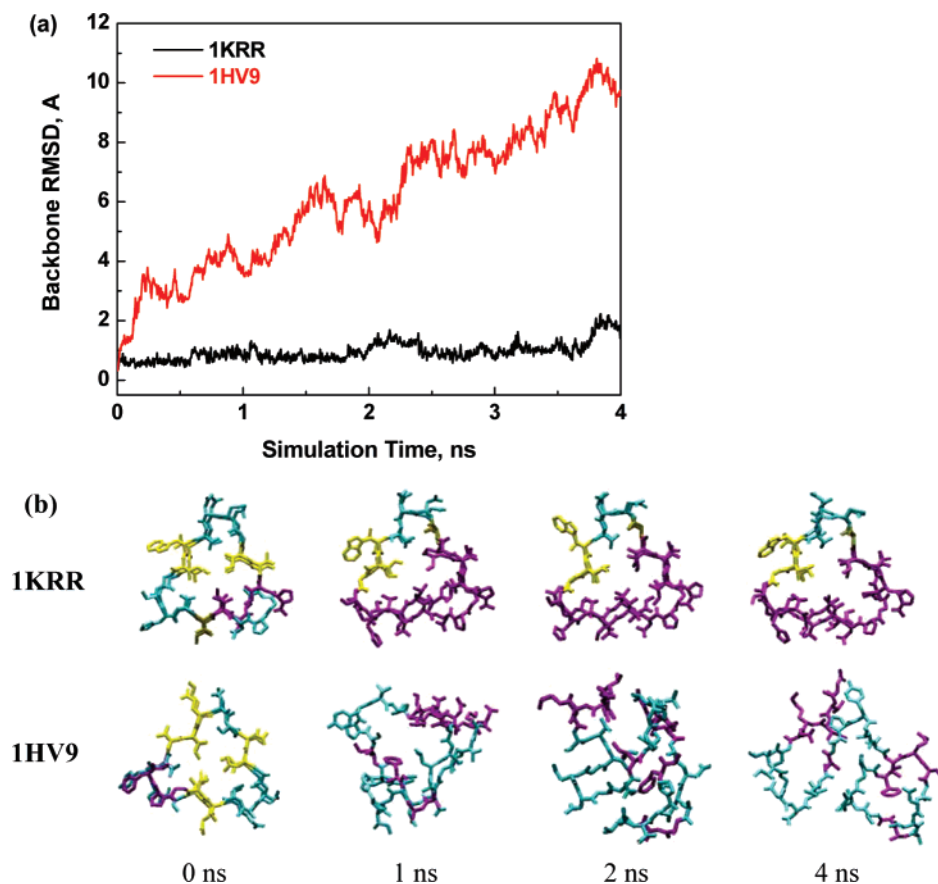


FIGURE 4: (a) Backbone RMSD of wild-type 1KRR (black) and 1HV9 (red) relative to their crystal structures as a function of simulation time at 330 K. (b) Snapshots of 1KRR (upper panel) and 1HV9 (lower panel) taken from the simulations at 0, 1, 2, and 4 ns, respectively. The coil is shown in purple, the turn in cyan, and the extension in yellow.

code, followed by its corresponding position number. For example, D10A27 signifies a double mutant with substitutions of Asp and Ala at positions 10 and 27 by Ac<sub>3</sub>c residues.

*Stability of the Single Unit of Wild-Type 1HV9 and 1KRR.* Figure 4a presents the backbone RMSDs of the peptides as compared to the initial crystal structure. These were calculated to measure the overall structural stability throughout the 4 ns simulations. For the wild-type 1KRR system, the backbone RMSD oscillated around a roughly constant value of  $1.0 \pm 0.2$  Å. No large conformational change was observed during the simulation, indicating that the overall structure of 1KRR was very stable (Figure 4b). Unlike 1KRR, the simulation of 1HV9 showed that within 0.25 ns the RMSD quickly increased to 3.5 Å and then gradually reached 10 Å at 4 ns, exhibiting a dramatic increase in fluctuation. The secondary structure, especially for the helical strand–loop motif, was no longer maintained as shown in a sequence of snapshots (Figure 4b). To assess the local dynamical variation of the peptides, the RMS fluctuation (RMSF) of individual C $\alpha$  atoms was measured from their average positions during the simulations (Figure 5a,b). The C $\alpha$  RMSF of the 1KRR structure displayed low fluctuation for all residues. In contrast, for 1HV9, two sharp peaks corresponding to loop L1 (residues Lys4, Asn5, and Ser6) and loop L2 (residues Ala26, Ala27, and Ala28) were observed. The  $\beta$ -strand regions exhibit significantly smaller fluctuations from their average positions than the loop regions. Comparison of the RMSD and RMSF indicates that the loop regions are the primary contributors to the overall instability in 1HV9.

Panels c and d of Figure 5 showed the  $(\varphi, \psi)$  distributions for loop residues of 1KRR and 1HV9, respectively. For 1KRR, the  $(\varphi, \psi)$  distributions in three loop regions fell into two clusters, one of which occurs in the  $\beta$  region and the other in the  $\alpha_L$  region, consistent with the experimental observation by Govaerts and co-workers (26) that, for left-handed  $\beta$ -helices, the residues in the loop regions mainly adopt  $\alpha_L$  conformations. In contrast, residues in the loop regions of 1HV9 exhibited larger backbone torsion variations in the  $\beta$  and  $\alpha_R$  regions with a wide range of  $\psi = -180^\circ$  to  $180^\circ$ . These findings suggest that the secondary structures of the loop regions in 1KRR are relatively well preserved as compared to those of 1HV9, consistent with the RMSD and RMSF results.

Figure 5e showed the evolution of the native contacts for both 1KRR and 1HV9. By decomposing the native contacts into backbone hydrogen bonds and side chain contacts, it can be seen that, for both 1KRR and 1HV9, a large number of side chain contacts remained approximately constant. On the other hand, the total number of backbone hydrogen bonds of 1HV9 dropped from the initial value of  $\sim 30$  to  $\sim 5$  within 0.5 ns and remained at this value for the rest of the simulation, whereas 1KRR maintained an almost constant number of backbone hydrogen bonds during the simulations. Moreover, 1KRR has only one negatively charged residue, Asp24, located at loop 3 (Figure 3). 1HV9 has six charged residues (Asp10, Asp11, Glu21, Asp22, Lys4, and Glu13), and two pairs of negatively charged, adjacent residues, Asp10–Asp11 and Glu21–Asp22, are in the flexible loop regions, which leads to unfavorable electrostatic repulsion,

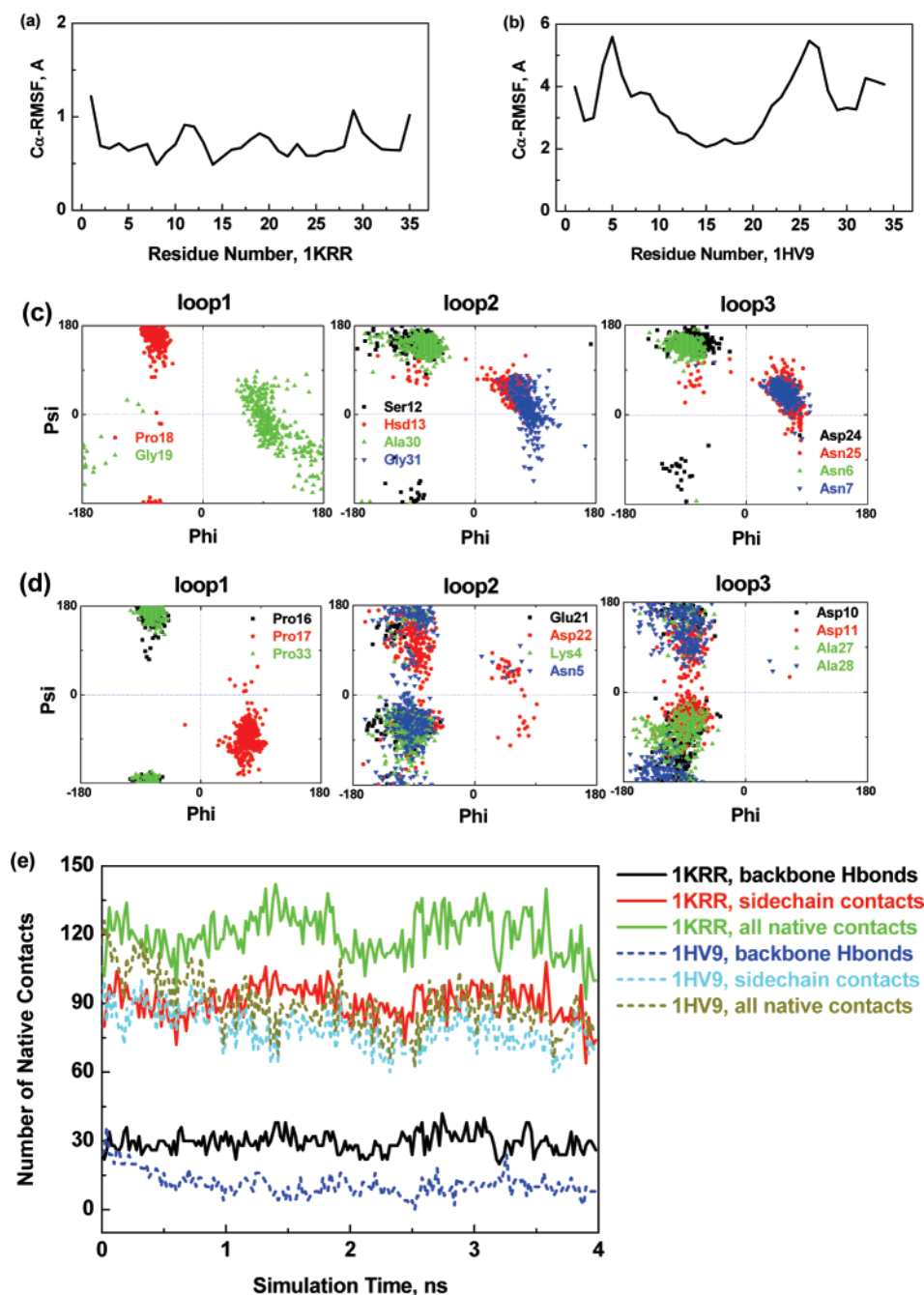


FIGURE 5: Residue-based C $\alpha$  RMSFs for wild-type (a) 1KRR and (b) 1HV9. Backbone torsion angle distributions for the loop residues in (c) 1KRR and (d) 1HV9. (e) Time-dependent native contacts of 1KRR and 1HV9, where native contacts consist of backbone hydrogen bonds and side chain native contacts.

destabilizing the peptide. Taken together, the structural instability of 1HV9 could be attributed to the loss of backbone hydrogen bonds and electrostatic repulsion of the charged side chains in the loop regions.

*Stability of the Single Unit of Mutants 1HV9 and 1KRR.* A residue was selected and mutated by Ac<sub>3</sub>C according to the following criteria: (i) The residue is located in the loop regions. The loop and turn regions generally display higher mobility because they are loosely packed against each other or against the  $\beta$ -sheets (68). Thus, targeting flexible regions could have direct impact on the structural stability of peptides. (ii) The side chain of the residue in the loop regions is outward-pointing away from the hydrophobic core. (iii) To reduce the electrostatic repulsion, a residue with charged

side chains in the loop regions could be a candidate position for substitution. (iv) The backbone conformation of the residue is not preferred to be in the  $\beta$ -strand. Preferably, the mutated residue should be able to participate in a  $\beta$ -turn within the loop in order to facilitate and stabilize the incorporation of the Ac<sub>3</sub>C residue.

For the 1KRR systems, the two double mutants of N7N25 and H13G31 were generally stable but exhibited small structural flexibility with RMSD values of  $\sim 1.0 \pm 0.1$  Å, close to the RMSD value of the wild type, while the single mutant A30 and double mutant S12A30 experienced larger structural deviations and were not able to maintain the native  $\beta$ -helical structures, as shown in Figure 6a. For the 1HV9 systems, the RMSDs of all mutants were smaller than that

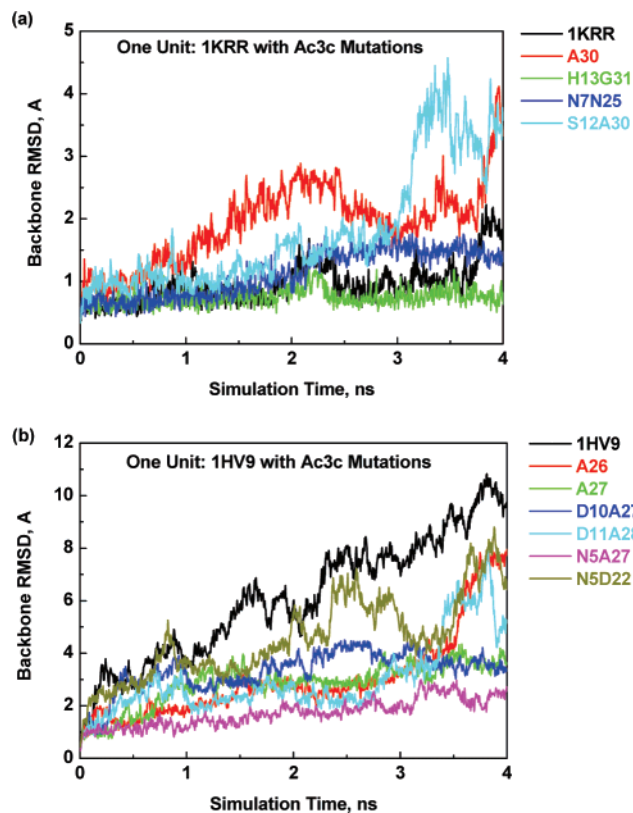


FIGURE 6: Backbone RMSD of (a) 1KRR mutants and (b) 1HV9 mutants.

of the wild type (Figure 6b). Among the mutants, the structural deviations for the mutants of N5A27, A27, and D10A27 were maintained at a relatively low level in the 4 ns simulations ( $<4$  Å). For the mutants of A26 and D11A28, the RMSDs gradually increased to 4 Å within the first 3.5 ns and then rapidly increased to 7 Å in the last 0.5 ns, indicating that a conformational change occurred at 3.5 ns. The least stable N5D22 mutant suffered substantial conformational changes with large RMSD fluctuations. Replacements of D10 or D11 by Ac<sub>3c</sub> have been shown to increase the stability by removal of the electrostatic repulsion between the negative charges of D10 and D11 in the loop region. We note however that RMSD values do not necessarily provide accurate insights into the structural changes. Visual inspection of all trajectories confirmed that Ac<sub>3c</sub> substitutions in the loop regions were able to enhance the stability of the  $\beta$ -helical structures to some extent. Although 1HV9 mutants N5D22, A26, and D11A28 were unstable, those mutants still exhibited structural stability during a longer time than the wild type. The increased stability could originate from the constrained local loop conformations as well as possible reduction in electrostatic repulsion.

Figure 7 shows the residue-based fluctuation of the mutants in comparison with their corresponding wild types. For all 1KRR mutants, Ac<sub>3c</sub> substitutions in the loop regions did not reduce the fluctuations of the residues. Although the Ac<sub>3c</sub> substitution could disrupt either the initial geometry (e.g., backbone conformation and side chain packing) or the extensive hydrogen bond network with neighboring residues, the Ac<sub>3c</sub> restrictions could also drag the peptide to the desired conformation without large structural distortion. Nevertheless, as compared with the unstable 1HV9 wild type, Ac<sub>3c</sub>

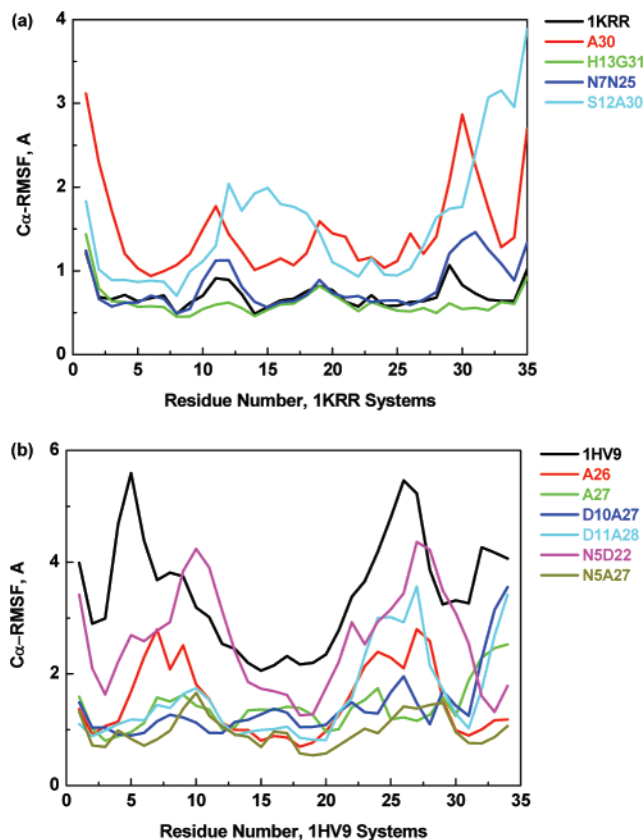


FIGURE 7: Residue-based C $\alpha$  RMSFs for (a) 1KRR mutants and (b) 1HV9 mutants in comparison with that of the corresponding wild type.

substitutions suppressed the structural fluctuations in the loop 1 and loop 2 regions, simply because of the introduction of backbone constraints. In particular, three mutants (A27, D10A27, and N5A27) exhibited the most dramatic reduction of residue fluctuations across the entire sequence. All three mutants involved a mutation at position Ala27. This observation may imply that this mutation site has substantial influence on residue flexibility and overall structural stability.

Figure 8 shows the backbone conformations of all residues in the loops for 1KRR mutant N7N25 and 1HV9 mutant A27. As can be seen, the backbone dihedral angles of Ac<sub>3c</sub> at substituted positions are restricted to  $\varphi \approx \pm 80^\circ$  and  $\psi \approx 0^\circ$ , consistent with both the intrinsic conformational preferences predicted for the isolated residue (45, 46) and the experimental data of small peptides containing this residue (45, 46). Although an Ac<sub>3c</sub> substitution could alter the backbone dihedral angles of its neighboring residues, overall the loop residues can self-adapt to the regular  $\beta$ -helical organization. As compared with wild types (Figure 5), the distribution of ( $\varphi$ ,  $\psi$ ) dihedral angles is narrowed in the mutants, simply because Ac<sub>3c</sub> restricts backbone conformation to the desired value and thus contributes to its structural stability.

*Stability of Nanotubular Structures.* As expected, during the 12 ns simulation the 1KRR nanotubular structure with four repeat units displayed a high stability with a small structural difference from the initial structure of about 1.1 Å (Figure 9). The 1KRR tubular model retained an approximately constant number of hydrogen bonds (Figure 11a) and hydrophobic contacts (Figure 12a) between adjacent

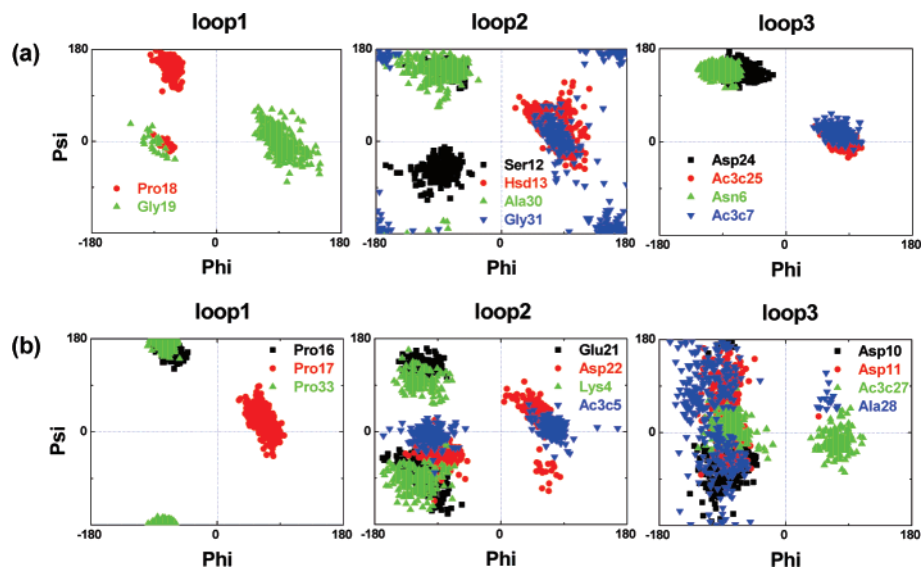


FIGURE 8: Backbone torsion angle ( $\varphi$ ,  $\psi$ ) distributions for the loop residues in the (a) 1KRR-N7N25 mutant and (b) 1HV9-A27 mutant.

subunits throughout the simulation, most of which were preserved. These hydrogen bonds and hydrophobic contacts might also contribute to the preservation of the intermolecular distance at its initial value of 9.8 Å (Figure 10a). The relatively constant intermolecular distance also indicates that each subunit has a fairly good backbone and side chain interactions with its neighbors. In contrast, the 1HV9 nanotubular structure displayed its instability with a continual increase in the structural fluctuation. Visual inspection (Figure 9c) showed that at 3 ns the subunits of 1HV9 started to move away from each other; at 6 ns two edge subunits were rotated and shifted, causing a bent nanotubular structure, and at the same time the intermolecular interface was largely exposed to bulk solvent; and at 12 ns 1HV9 completely lost the initial, compact nanotubular structure. During the disassociation process, the 1HV9 tubular model exhibited a rapid increase in the averaged intermolecular distance. It appears that the loss of hydrogen bonds (Figure 11b) and hydrophobic contacts (Figure 12b) between the subunit building blocks are responsible for the nanostructure disassociation.

For the 1KRR mutant systems, the structural deviation for the H13G31 mutant was among the largest. The backbone RMSD continued to rise during the 12 ns simulation to reach 5.5 Å relative to the starting structure (Figure 9a). This behavior is consistent with the intermolecular distance between each subunit building block increasing from the initial value of 9.8 to 12.5 Å (Figure 10a). The instability of this nanostructure could be partially attributed to the loss of hydrogen bonds and hydrophobic contacts between each subunit (Figures 11a and 12a). In addition, substitution of the flexible Gly31 by the rigid Ac<sub>3</sub>c in the loop motif Gly29-Ala30-Gly31 would result in a steric conflict with its neighboring residues Ala30 and Ser32. Substituted Ac<sub>3</sub>c may not allow a conformational adjustment for favorable vdW interactions with its neighboring residues. In contrast, the structural deviations for other 1KRR mutants were maintained at relatively stable plateaus, ranging from 2 to 4 Å, without a significant drift throughout the simulations. The RMSD profiles together with a visual inspection of the snapshots (Figure 9c) and the geometrical characterization, i.e., the intermolecular distances (Figure 10a), showed that

the overall tubular structures remained stable. All 1KRR mutants, especially the polar residues (His13, Ser12, Asn7, and Asn25), experienced structural changes which are larger than those observed for the wild type. This is since 1KRR itself and its nanostructure were relatively stable, implying that the intra- and interbuilding block interactions arising from such side chain contacts, backbone hydrogen bonding, electrostatic interactions, and geometrical stacking were already optimized by nature. Although Ac<sub>3</sub>c substitutions in loop regions may disrupt these, Ac<sub>3</sub>c can compensate by restricting the conformational freedom and optimizing in the new environment.

For the 1HV9 mutant systems, mutant Ala26 lost its tubular organization at a very early stage of the simulation, as evidenced by the remarkably large RMSD and the intersubunit distance. Since Ala26 was located in the  $\beta$ -strand position where it connected Leu25 in the  $\beta$ -strand region and Ala27 in the loop 2 region, Ac<sub>3</sub>c replacement at this position not only failed to provide strong backbone restriction in the loop 2 region but also disrupted the local backbone conformation in the  $\beta$ -strand region, thus leading to disassociation as the wild type did. Other 1HV9 mutants, after appropriate equilibration, were able to maintain their initial tubular structures with relatively low structural deviations in the range of 2–4 Å during 12 ns. The analysis of the mass center distance between subunit building blocks also confirmed this observation (Figure 10b). Compared to the wild-type tubular structure, the enhanced stability originates not only from the increasing number of hydrogen bonds and hydrophobic contacts between each building subunit (Figures 11b and 12b) but also from the reduced flexibility in the loop regions induced by Ac<sub>3</sub>c within each building subunit. Between the subunits, the hydrogen bonds and hydrophobic interactions help to hold the entire tubular structure together, while within the building subunit, substituted Ac<sub>3</sub>c in the loop regions help to retain the secondary structure conformation especially for the loop-strand motif.

*Stability of 1KRR Trimeric Structures.* In the native protein fold, 1KRR contains three  $\beta$ -helical segments forming a trimeric structure along a 3-fold screw axis (63). We performed additional simulations to investigate the stability

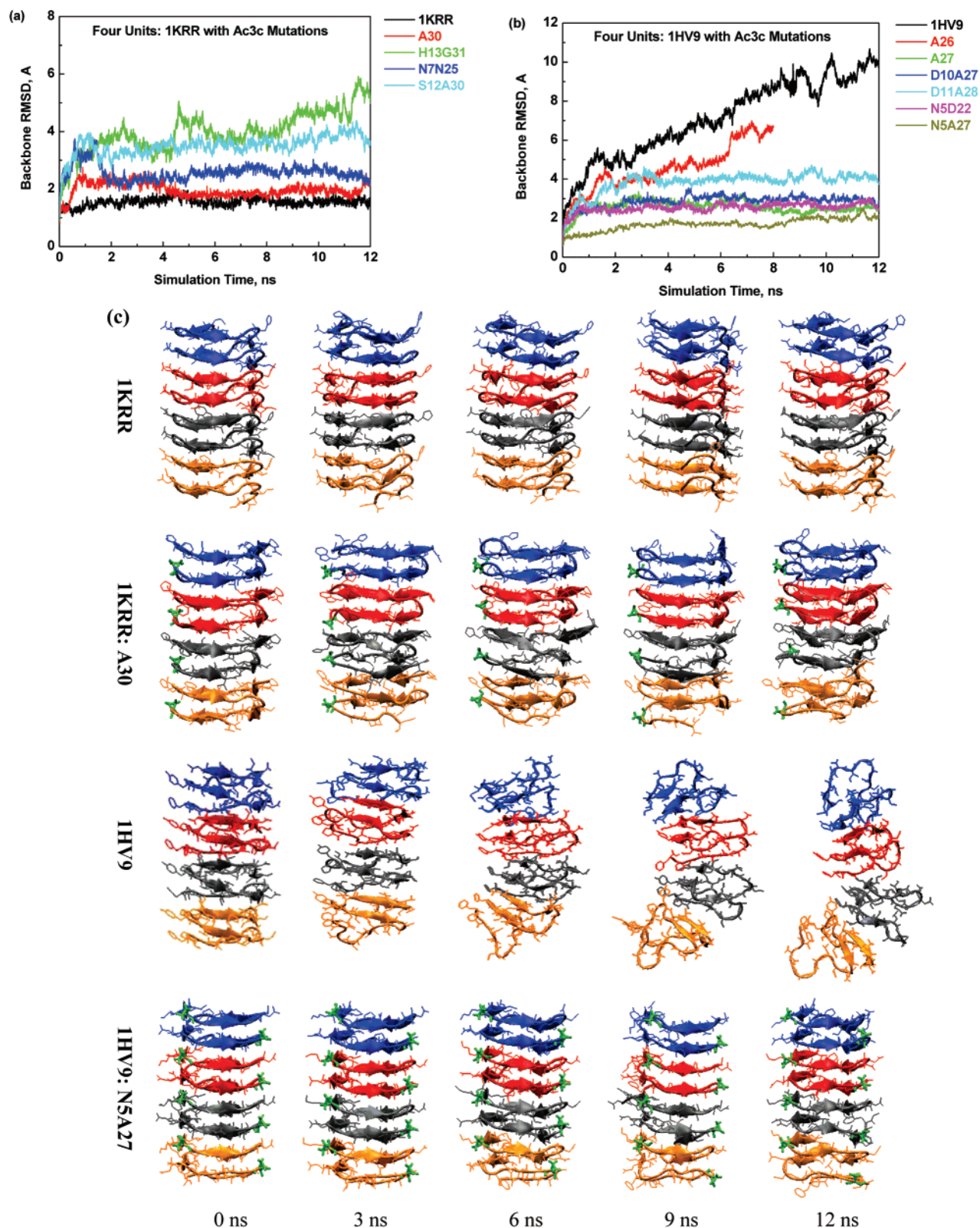


FIGURE 9: Backbone RMSD of (a) 1KRR and (b) 1HV9 nanotubular systems. (c) Snapshots of 1KRR, 1KRR-A30, 1HV9, and 1HV9-N5A27 from the simulations taken at 0, 3, 6, 9, and 12 ns, respectively. Ac3c is displayed as a green stick.

of 1KRR trimeric structures with single and four repeat units for the wild-type and mutated sequences. For the four repeat units, we observed that the overall size of the trimeric structures as measured by  $R_{\text{gyr}}$  was very stable, with around  $20.3 \pm 0.2$  Å for different sequences. As compared to monomeric structures (Figure 9a), trimeric structures have relatively small structural deviation from their starting

structures, with the RMSD values oscillating around  $1.3 \pm 0.2$  Å. Thus, both RMSD and radius of gyration values consistently showed that the trimeric structures have a higher stability than the monomeric structures, mainly because trimeric structures have a much larger interface involving three  $\beta$ -helical segments. Mutations occurring at the sub- $\beta$ -unit interfaces did not improve the overall stability of trimeric

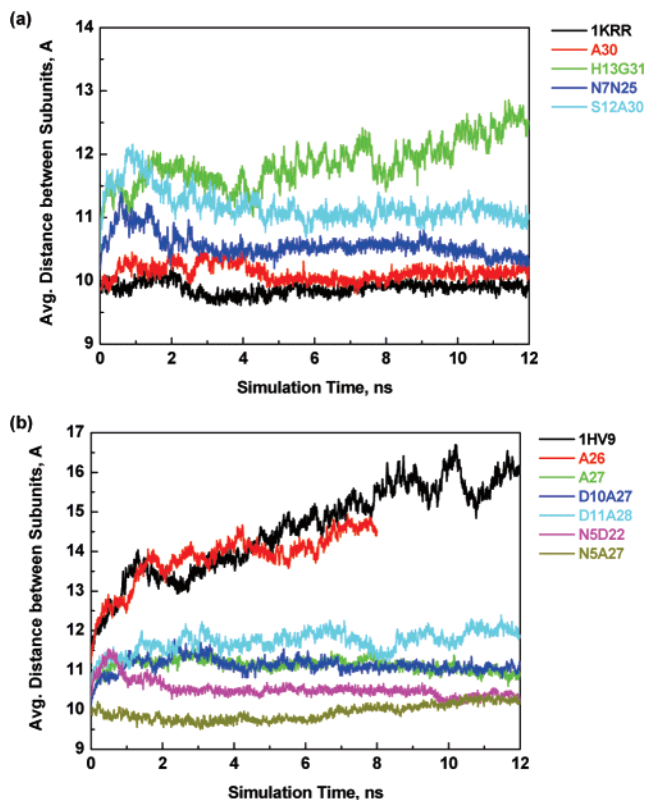


FIGURE 10: Time evolution of the average mass center distance between adjacent building subunits for (a) 1KRR and (b) 1HV9 nanotubular systems.

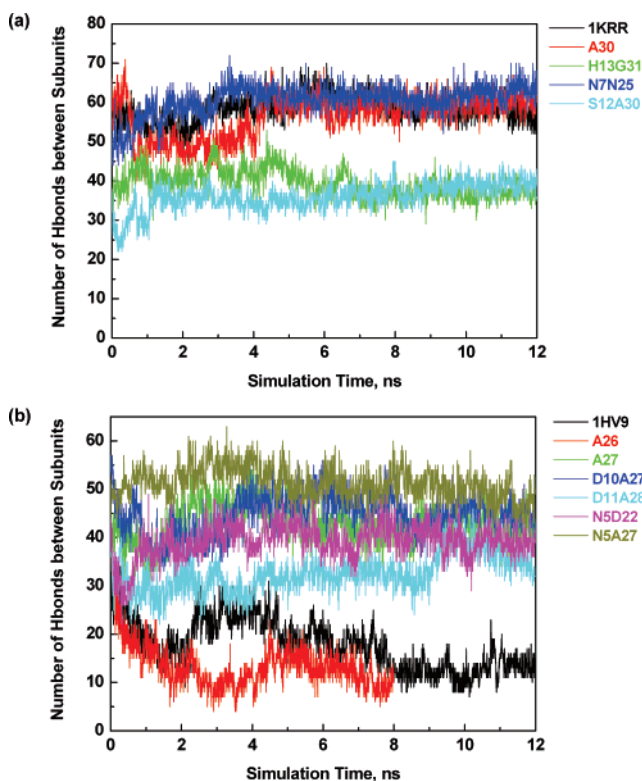


FIGURE 11: Time evolution of the total number of hydrogen bonds between adjacent building subunits in (a) 1KRR and (b) 1HV9 nanotubular systems.

structures (Figure 13a). But the original triangular form was well maintained during the simulations (Figure 13c), implying that the monomeric 1KRR triangular form could be the

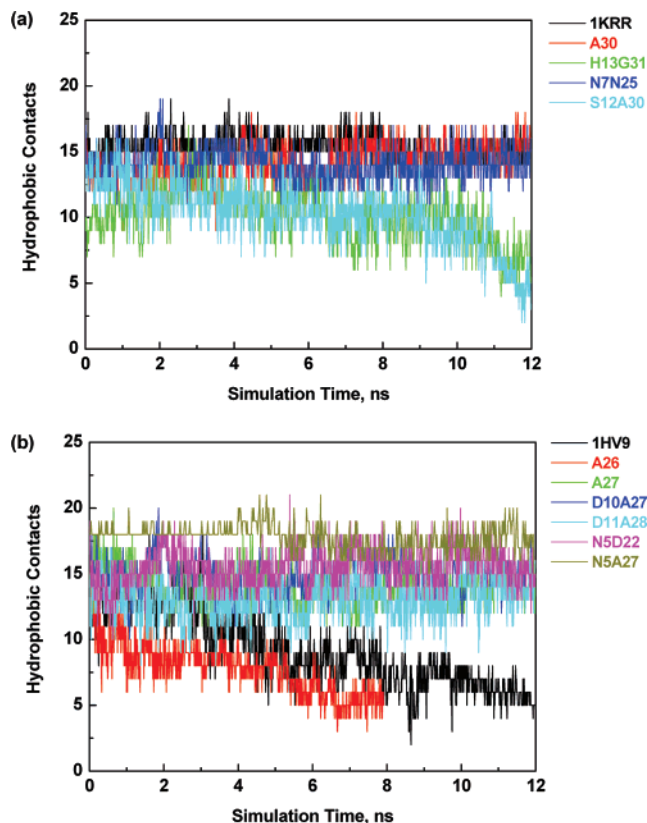


FIGURE 12: Time evolution of the total number of hydrophobic contacts between adjacent building subunits for (a) 1KRR and (b) 1HV9 nanotubular systems.

native state. We note, however, that for the single repeat unit all trimeric structures were unstable. The three  $\beta$ -helical segments separated from each other very quickly, but each of them was still well conserved (data not shown). Similar to amyloid fibril elongation, the stability of trimeric structures increased as they progressed along a 3-fold screw axis.

## DISCUSSION

For the left-handed  $\beta$ -helical nanotubular structures in this study,  $Ac_3c$  substitutions in loop regions generally enhance the overall stability of the nanostructure. Simulation results also show that the stability is position-dependent. Some positions are very tolerant to mutations, while others are sensitive. Detailed analysis of the interactions between protein building blocks is crucial to understand the structural basis of stabilization/destabilization effects.

*Association Force.* In general, the driving force for molecular assembly is mainly based on electrostatic attraction, vdW interactions, hydrophobic interactions, and hydrogen bonds, that is, geometric complementarity and structural compatibility (69). Comparing the structural stability of a single building subunit with that of four subunits for the 1KRR and 1HV9 systems, it appears that extra building units could delay the progressive loss of the organization. The stacking of identical residues on top of each other, for example, Asn-Asn ladders occurring in the nanotubular structures, provides additional stability to the nanostructures. Furthermore, association forces such as hydrogen bonds and hydrophobic contacts between adjacent subunits also contribute to the stability of the nanostructures. The intermolecular interactions between subunits may com-

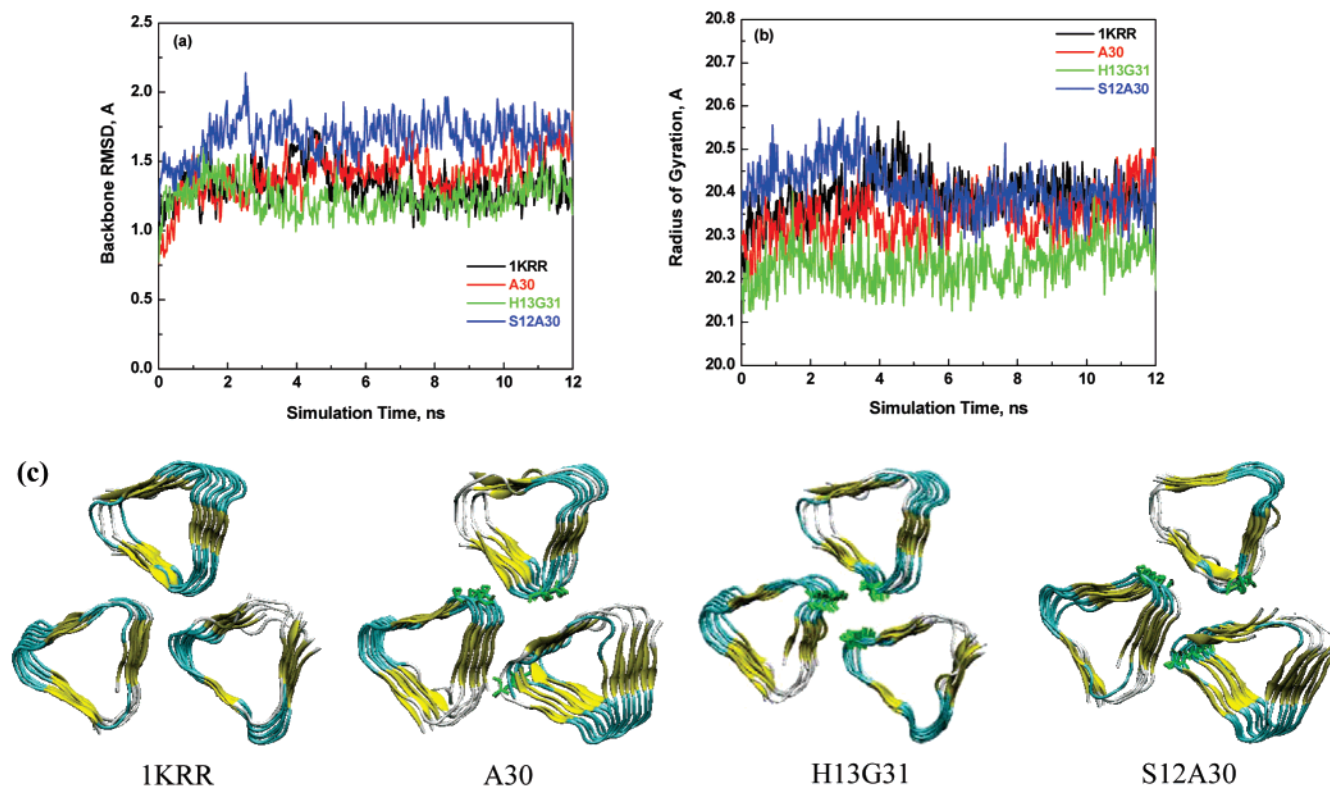


FIGURE 13: Evolution of the 1KRR trimeric structures during the simulations. (a) Backbone RMSD, (b) radius of gyration, and (c) snapshots of wild-type 1KRR and its mutant (i.e., A30, H13G31, and S12A30) from the simulations at 12 ns. Ac<sub>3</sub>c is displayed as a green stick.

pensate for some of the local structural changes that destabilize the monomeric building blocks. Even for the unstable nanotubular structures that tend to disassociate at a very early stage of the simulations, the disruption of the loop-strand motif is slowed down, and the subunits in the middle continued to be rather stable. This is not surprising: associations through noncovalent interactions between the building blocks mutually stabilize each other due to the increased interactions at the interfaces. Similar stabilizing behavior was also observed in other protein and peptide assemblies. For example, higher order aggregates of amyloid fibrils generally exhibit more stable molecular structures (39, 70), with the stability increasing with size.

**Molecular Size and Hydrophobicity.** For a successful design, it is desirable that the substitutions retain both favorable packing interactions and hydrogen bonding with the neighboring residues. A large substituted residue would lead to unfavorable steric hindrance with nearby residues while a small one cannot attain sufficient packing interactions. The hydrophobic, small alanine is a suitable amino acid to be replaced by Ac<sub>3</sub>c since it has a comparable size and hydrophobicity with respect to Ac<sub>3</sub>c. Ala stabilizes the nanotubular structures at position 30 in the Gly29-Ala30-Gly31 motif of the 1KRR system and at position 27 in the Ala26-Ala27-Ala28 motif of the 1HV9 system, respectively. On the other hand, the replacement of large, polar residues by Ac<sub>3</sub>c leads to the loss of hydrogen bonds and side chain interactions with the neighboring residues. Simulation results showed that most of the mutants with substitutions of polar, hydrophilic residues (Asn, His, and Gln) by Ac<sub>3</sub>c in both 1KRR and 1HV9 systems exhibited relatively stable nanotubular structures, but they were not as stable as the mutants with replacement of Ala → Ac<sub>3</sub>c. This fact indicates that, as

compared to the reduction of flexibility in the loop region by the introduction of the highly constrained Ac<sub>3</sub>c, the loss of hydrogen bonds and side chain contacts does not necessarily destabilize the nanostructure.

We also examined the effect of c<sub>3</sub>Dip substitutions on the stability of single building subunits and on the stability of four repetitive subunits of 1KRR and 1HV9 systems (data not shown). The mutation sites were exactly the same as those in Ac<sub>3</sub>c studies. Simulations showed that for both 1KRR and 1HV9 systems, c<sub>3</sub>Dip mutants with a single building subunit experienced relatively larger structural deviations than Ac<sub>3</sub>c mutants while still maintaining the native triangular conformation to some extent. However, none of the mutants was able to maintain the initial tubular structures, and they disassociated quickly, especially for those double mutants in which mutations occur at two consecutive loop positions. This could be due to the large c<sub>3</sub>Dip residues with two phenylalanine rings which cannot properly fit in the tightly packed loop regions to avoid steric conflict with neighboring residues and neighboring subunits while still maintaining favorable interactions such as hydrogen bonding and  $\pi$ -stacking interactions. These results indicate that synthetic amino acids must be engineered, taking into account not only the desired conformational motif but also the steric and geometric restrictions imposed by the molecular system where it will be incorporated. Accordingly, the stereochemical constraints designed to stabilize a given region of the conformational map should reflect this equilibrium. The size of c<sub>3</sub>Dip, originally designed to stabilize the  $\gamma$ -turns in small model peptides (53), may not be suitable for the  $\beta$ -helical structures.

**Mutation Site.** The reduction of loop flexibility may increase the population time of the peptide in the proper

conformation prior to assembly. Our results suggest that residues in the  $\beta$ -strand region are more sensitive to Ac<sub>3</sub>c replacement, as shown in the case of the A26 mutant in the 1HV9 system. Ac<sub>3</sub>c replacement in this site fails to maintain the proper fold of the peptide and to reduce the conformational flexibility of the loop, leading to the large structural deviation. In addition, Gly occurring in the loop region would not be a good candidate to be substituted by Ac<sub>3</sub>c to enhance the stability. Gly has a high occurrence in the turn or loop region, where it acts as a flexible hinge to absorb the tension in the loop. Its flexible backbone allows a conformational adjustment to avoid steric hindrance with its adjacent residues while still maintaining favorable interactions. A sterically unfavorable substitution of Gly by an Ac<sub>3</sub>c residue would weaken the hinge activity due to improper backbone geometry, as indicated in the 1KRR-H13G31 nanostructure.

## CONCLUSIONS

In this work, we construct novel nanotubular structures by stacking left-handed  $\beta$ -helical protein building blocks on top of each other. We focus on two left-handed  $\beta$ -helical motifs. A conformationally constrained synthetic residue (Ac<sub>3</sub>c) is introduced in the loop regions to examine the effect of a geometrical confinement on the stability of nanotubular structures. All-atom MD simulations show that when Ac<sub>3</sub>c is introduced in the loop regions, it is able to enhance the stability of the nanotubular structures due to its highly strained backbone and strong tendency to adopt a turn structure. This is consistent with our earlier computational studies, which used the native amino acid proline to improve the stability of the nanostructure (44). Position-specific mutations also indicate that a potentially good mutational site should have comparable molecular size, proper backbone geometry, and similar hydrophobicity with respect to those properties of Ac<sub>3</sub>c. Specifically, substitutions of the middle Ala by Ac<sub>3</sub>c in different Gly-Ala-Gly and Ala-Ala-Ala motifs lead to remarkable stability, implying that these motifs could be potential targets for mutations. To further address the potential use of conformationally restricted amino acids to stabilize natural building block foldamers, we are currently exploring other 1-aminocycloalkanecarboxylic analogues (Ac<sub>*n*</sub>c with *n* = 4, 5, or 6, where *n* represents the size of the cyclic side chain) to examine their stabilizing effect on nanostructures using both experimental and computational techniques.

## ACKNOWLEDGMENT

We thank Drs. B. Ma and Y. Pan for many useful comments and suggestions. The authors are grateful to the high-performance computational capabilities of the Biowulf PC/Linux cluster at the National Institutes of Health, Bethesda, MD (<http://biowulf.nih.gov>) and to the BSC (Barcelona Supercomputer Center) for the access to the Marenostrum supercomputer.

## REFERENCES

- Tovar, J. D., Claussen, R. C., and Stupp, S. I. (2005) Probing the interior of peptide amphiphile supramolecular aggregates, *J. Am. Chem. Soc.* *127*, 7337–7345.
- Reches, M., and Gazit, E. (2003) Casting metal nanowires within discrete self-assembled peptide nanotubes, *Science* *300*, 625–627.
- Zhang, S. (2003) Fabrication of novel biomaterials through molecular self-assembly, *Nat. Biotechnol.* *21*, 1171–1178.
- Percec, V., Dulcey, A. E., Peterca, M., Ilies, M., Sienkowska, M. J., and Heiney, P. A. (2005) Programming the internal structure and stability of helical pores self-assembled from dendritic dipeptides via the protective groups of the peptide, *J. Am. Chem. Soc.* *127*, 17902–17909.
- Ivanov, I., Vemparala, S., Pophristic, V., Kuroda, K., DeGrado, W. F., McCammon, J. A., and Klein, M. L. (2006) Characterization of nonbiological antimicrobial polymers in aqueous solution and at water-lipid interfaces from all-atom molecular dynamics, *J. Am. Chem. Soc.* *128*, 1778–1779.
- Lee, C. C., MacKay, J. A., Frechet, J. M. J., and Szoka, F. C. (2005) Designing dendrimers for biological applications, *Nat. Biotechnol.* *23*, 1517–1526.
- Rajagopal, K., and Schneider, J. P. (2004) Self-assembling peptides and proteins for nanotechnological applications, *Curr. Opin. Struct. Biol.* *14*, 480–486.
- Adler-Abramovich, L., Reches, M., Sedman, V. L., Allen, S., Tendler, S. J. B., and Gazit, E. (2006) Thermal and chemical stability of diphenylalanine peptide nanotubes: implications for nanotechnological applications, *Langmuir* *22*, 1313–1320.
- Song, Y., Challa, S. R., Medforth, C. J., Qiu, Y., Watt, R. K., Peña, D., Miller, J. E., Swol, F. v., and Shelmutt, J. A. (2004) Synthesis of peptide-nanotube platinum-nanoparticle composites, *Chem. Commun.* *9*, 1044–1045.
- Vauthey, S., Santoso, S., Gong, H., Watson, N., and Zhang, S. (2002) Molecular self-assembly of surfactant-like peptides to form nanotubes and nanovesicles, *Proc. Natl. Acad. Sci. U.S.A.* *99*, 5355–5360.
- Yokoi, H., Kinoshita, T., and Zhang, S. (2005) Dynamic reassembly of peptide RADA16 nanofiber scaffold, *Proc. Natl. Acad. Sci. U.S.A.* *102*, 8414–8419.
- Li, S., Hill, C. P., Sundquist, W. I., and Finch, J. T. (2000) Image reconstructions of helical assemblies of the HIV-1 CA protein, *Nature* *407*, 409–413.
- Tsai, C.-J., Zheng, J., and Nussinov, R. (2006) Designing a nanotube using naturally occurring protein building blocks, *PLoS Comput. Biol.* *2*, e42.
- Tsai, C.-J., Maizel, J. V., Jr., and Nussinov, R. (2000) Anatomy of protein structures: visualizing how a one-dimensional protein chain folds into a three-dimensional shape, *Proc. Natl. Acad. Sci. U.S.A.* *97*, 12038–12043.
- Tsai, H.-H., Tsai, C.-J., Ma, B., and Nussinov, R. (2004) In silico protein design by combinatorial assembly of protein building blocks, *Protein Sci.* *13*, 2753–2765.
- Main, E. R. G., Lowe, A. R., Mochrie, S. G. J., Jackson, S. E., and Regan, L. (2005) A recurring theme in protein engineering: the design, stability and folding of repeat proteins, *Curr. Opin. Struct. Biol.* *15*, 464–471.
- Kajander, T., Cortajarena, A. L., Main, E. R. G., Mochrie, S. G. J., and Regan, L. (2005) A new folding paradigm for repeat proteins, *J. Am. Chem. Soc.* *127*, 10188–10190.
- Main, E. R. G., Stott, K., Jackson, S. E., and Regan, L. (2005) Local and long-range stability in tandemly arrayed tetratricopeptide repeats, *Proc. Natl. Acad. Sci. U.S.A.* *102*, 5721–5726.
- Kobe, B., and Kajava, A. V. (2000) When protein folding is simplified to protein coiling: the continuum of solenoid protein structures, *Trends Biochem. Sci.* *25*, 509–515.
- Mello, C. C., and Barrick, D. (2004) An experimentally determined protein folding energy landscape, *Proc. Natl. Acad. Sci. U.S.A.* *101*, 14102–14107.
- Bell, J. K., Botos, I., Hall, P. R., Askins, J., Shiloach, J., Segal, D. M., and Davies, D. R. (2005) The molecular structure of the Toll-like receptor 3 ligand-binding domain, *Proc. Natl. Acad. Sci. U.S.A.* *102*, 10976–10980.
- Padilla, J. E., Colovos, C., and Yeates, T. O. (2001) Nanohedra: Using symmetry to design self assembling protein cages, layers, crystals, and filaments, *Proc. Natl. Acad. Sci. U.S.A.* *98*, 2217–2221.
- Alemán, C., Zanuy, D., Jiménez, A. I., Cativiela, C., Haspel, N., Zheng, J., Casanovas, J., Wolfson, H., and Nussinov, R. (2006) Concepts and schemes for the re-engineering of physical protein

- modules: generating nanodevices via targeted replacements with constrained amino acids, *Phys. Biol.* 3, S54–S62.
24. Leinala, E. K., Davies, P. L., and Jia, Z. (2002) Crystal structure of [beta]-helical antifreeze protein points to a general ice binding model, *Structure* 10, 619–627.
25. Pye, V. E., Tingey, A. P., Robson, R. L., and Moody, P. C. E. (2004) The structure and mechanism of serine acetyltransferase from *Escherichia coli*, *J. Biol. Chem.* 279, 40729–40736.
26. Govaerts, C., Wille, H., Prusiner, S. B., and Cohen, F. E. (2004) Evidence for assembly of prions with left-handed beta-helices into trimers, *Proc. Natl. Acad. Sci. U.S.A.* 101, 8342–8347.
27. Sharma, G. V. M., Reddy, K. R., Krishna, P. R., Sankar, A. R., Jayaprakash, P., Jagannadh, B., and Kunwar, A. C. (2004) Left-handed helical twists in “mixed beta-peptides” derived from alternating c-linked carbo-beta-amino acids and beta-hGly units, *Angew. Chem., Int. Ed.* 43, 3961–3965.
28. Kreisberg, J. F., Betts, S. D., and King, J. (2000) Beta-helix core packing within the triple-stranded oligomerization domain of the P22 tailspike, *Protein Sci.* 9, 2338–2343.
29. Adzhubei, A. A., and Sternberg, M. J. E. (1993) Left-handed polypyrrolone II helices commonly occur in globular proteins, *J. Mol. Biol.* 229, 472–493.
30. Kostrewa, D., D’Arcy, A., Takacs, B., and Kamber, M. (2001) Crystal structures of *Streptococcus pneumoniae* N-acetylglucosamine-1-phosphate uridylyltransferase, GlmU, in apo form at 2.33 Å resolution and in complex with UDP-N-Acetylglucosamine and Mg<sup>2+</sup> at 1.96 Å resolution, *J. Mol. Biol.* 305, 279–289.
31. Sugantino, M., and Roderick, S. L. (2002) Crystal structure of vat(D): an acetyltransferase that inactivates streptogramin group A antibiotics, *Biochemistry* 41, 2209–2216.
32. Iverson, T. M., Alber, B. E., Kisker, C., Ferry, J. G., and Rees, D. C. (2000) A closer look at the active site of gamma-class carbonic anhydrases: high-resolution crystallographic studies of the carbonic anhydrase from *Methanosarcina thermophila*, *Biochemistry* 39, 9222–9231.
33. Beaman, T. W., Sugantino, M., and Roderick, S. L. (1998) Structure of the hexapeptide xenobiotic acetyltransferase from *Pseudomonas aeruginosa*, *Biochemistry* 37, 6689–6696.
34. Beaman, T. W., Blanchard, J. S., and Roderick, S. L. (1998) The conformational change and active site structure of tetrahydrodipicolinate N-succinyltransferase, *Biochemistry* 37, 10363–10369.
35. Jenkins, J., Mayans, O., and Pickersgill, R. (1998) Structure and evolution of parallel [beta]-helix proteins, *J. Struct. Biol.* 122, 236–246.
36. Guo, J.-t., Wetzel, R., and Xu, Y. (2004) Molecular modeling of the core of Abeta amyloid fibrils, *Proteins: Struct., Funct., Bioinf.* 57, 357–364.
37. Zanuy, D., Ma, B., and Nussinov, R. (2003) Short peptide amyloid organization: stabilities and conformations of the islet amyloid peptide NFGAIL, *Biophys. J.* 84, 1884–1894.
38. Zanuy, D., Gunasekaran, K., Lesk, A. M., and Nussinov, R. (2006) Computational study of the fibril organization of polyglutamine repeats reveals a common motif identified in [beta]-helices, *J. Mol. Biol.* 358, 330–345.
39. Zheng, J., Ma, B., Tsai, C.-J., and Nussinov, R. (2006) Structural stability and dynamics of an amyloid-forming peptide GNNQQNY from the yeast prion sup-35, *Biophys. J.* 91, 824–833.
40. Tsai, H.-H., Zanuy, D., Haspel, N., Gunasekaran, K., Ma, B., Tsai, C.-J., and Nussinov, R. (2004) The stability and dynamics of the human calcitonin amyloid peptide DFNKF, *Biophys. J.* 87, 146–158.
41. Chipot, C., and Tarek, M. (2006) Interaction of a peptide nanotube with a water-membrane interface, *Phys. Biol.* 3, S20–S25.
42. Beke, T., Czajlik, A., Csizmadia, I. G., and Perczel, A. (2006) Determining suitable lego-structures to estimate stability of larger peptide nanostructures using computational methods, *Phys. Biol.* 3, S26–S39.
43. Zheng, J., Li, L., Tsao, H.-K., Sheng, Y.-J., Chen, S., and Jiang, S. (2005) Strong repulsive forces between protein and oligo (ethylene glycol) self-assembled monolayers: a molecular simulation study, *Biophys. J.* 89, 158–166.
44. Haspel, N., Zanuy, D., Aleman, C., Wolfson, H., and Nussinov, R. (2006) De novo tubular nanostructure design based on self-assembly of [beta]-helical protein motifs, *Structure* 14, 1137–1148.
45. Alemán, C., Casanovas, J., and Galembeck, S. E. (1998) PAPQMD parametrization of molecular systems with cyclopropyl rings: conformational study of homopeptides constituted by 1-aminocyclopropane-1-carboxylic acid, *J. Comput.-Aided Mol. Des.* 12, 259–273.
46. Gomez-Catalan, J., Aleman, C., and Perez, J. J. (2000) Conformational profile of 1-aminocyclopropanecarboxylic acid, *Theor. Chem. Acc.* 103, 380–389.
47. Aleman, C. (1997) Conformational properties of [alpha]-amino acids disubstituted at the [alpha]-carbon, *J. Phys. Chem. B* 101, 5046–5050.
48. Fabiano, N., Valle, G., Crisma, M., Toniolo, C., Saviano, M., Lombardi, A., Isernia, C., Pavone, V., Di Blasio, B., Pedone, C., and Benedetti, E. (1993) Conformational versatility of the N-alpha-acylated tripeptide amide tail of oxytocin—synthesis and crystallographic characterization of 3C-2-alpha-backbone modified, conformationally restricted analogs, *Int. J. Pept. Protein Res.* 42, 459–465.
49. Valle, G., Crisma, M., Toniolo, C., Holt, E. M., Tamura, M., Bland, J., and Stamimer, C. H. (1989) Linear oligopeptides. 200. Crystallographic characterization of conformation of 1-aminocyclopropane-1-carboxylic acid residue (Ac<sub>3</sub>C) in simple derivatives and peptides, *Int. J. Pept. Protein Res.* 34, 56–65.
50. Benedetti, E., Di Blasio, B., Pavone, V., Pedone, C., Santini, A., Barone, V., Fraternali, F., Lelj, F., Baboso, A., Crisma, M., and Toniolo, C. (1989) Linear oligopeptides. 202. Structural versatility of peptides containing C-alpha-alpha-dialkylated glycines—An X-ray diffraction study of 6 1-aminocyclopropane-1-carboxylic acid rich peptides, *Int. J. Biol. Macromol.* 11, 353–360.
51. Benedetti, E., Di Blasio, B., Pavone, V., Pedone, C., Santini, A., Crisma, M., Valle, G., and Toniolo, C. (1989) Structural versatility of peptides from C[alpha, alpha] dialkylated glycines: Linear Ac<sub>3</sub>C homo-oligopeptides, *Biopolymers* 28, 175–184.
52. Aleman, C., Jimenez, A. I., Cativiela, C., Perez, J. J., and Casanovas, J. (2002) Influence of the phenyl side chain on the conformation of cyclopropane analogues of phenylalanine, *J. Phys. Chem. B* 106, 11849–11858.
53. Toniolo, C., Crisma, M., Formaggio, F., and Peggion, C. (2001) Control of peptide conformation by the Thorpe-Ingold effect (C-alpha-tetrasubstitution), *Biopolymers* 60, 396–419.
54. Hruby, V. J., Li, G. G., Haskell Luevano, C., and Shenderovich, M. (1997) Design of peptides, proteins, and peptidomimetics in chi space, *Biopolymers* 43, 219–266.
55. Jimenez, A. I., Cativiela, C., and Marraud, M. (2000) A gamma-turn induced by a highly constrained cyclopropane analogue of phenylalanine (c(3)diPhe) in the solid state, *Tetrahedron Lett.* 41, 5353–5356.
56. Jimenez, A. I., Vanderesse, R., Marraud, M., Aubry, A., and Cativiela, C. (1997) Folding types of dipeptides containing the diastereoisomeric cyclopropanic analogues of phenylalanine, *Tetrahedron Lett.* 38, 7559–7562.
57. Jimenez, A. I., Cativiela, C., Aubry, A., and Marraud, M. (1998) Beta-turn preferences induced by 2,3-methanophenylalanine chirality, *J. Am. Chem. Soc.* 120, 9452–9459.
58. Casanovas, J., Jimenez, A. I., Cativiela, C., Perez, J. J., and Aleman, C. (2003) N-Acetyl-N'-methylamide derivative of (2S,3S)-1-amino-2,3-diphenylcyclopropanecarboxylic acid: Theoretical analysis of the conformational impact produced by the incorporation of the second phenyl group to the cyclopropane analogue of phenylalanine, *J. Org. Chem.* 68, 7088–7091.
59. Jiménez, A. I., Ballano, G., and Cativiela, C. (2005) First observation of two consecutive gamma turns in a crystalline linear dipeptide, *Angew. Chem., Int. Ed.* 44, 396–399.
60. Casanovas, J., Jimenez, A. I., Cativiela, C., Perez, J. J., and Aleman, C. (2006) Conformational analysis of a cyclopropane analogue of phenylalanine with two geminal phenyl substituents, *J. Phys. Chem. B* 110, 5762–5766.
61. Royo, S., DeBorggraeve, W. M., Peggion, C., Formaggio, F., Crisma, M., Jimenez, A. I., Cativiela, C., and Toniolo, C. (2005) Turn and helical peptide handedness governed exclusively by side-chain chiral centers, *J. Am. Chem. Soc.* 127, 2036–2037.
62. Crisma, M., De Borggraeve, W., Peggion, C., Formaggio, F., Royo, S., Jimenez, A. I., Cativiela, C., and Toniolo, C. (2006) Preferred 3D-structure of peptides rich in a severely conformationally restricted cyclopropane analogue of phenylalanine, *Chem. Eur. J.* 12, 251–260.

63. Wang, X.-G., Olsen, L. R., and Roderick, S. L. (2002) Structure of the lac operon galactoside acetyltransferase, *Structure* 10, 581–588.
64. Olsen, L. R., and Roderick, S. L. (2001) Structure of the *Escherichia coli* GlmU pyrophosphorylase and acetyltransferase active sites, *Biochemistry* 40, 1913–1921.
65. Kale, L., Skeel, R., Bhandarkar, M., Brunner, R., Gursoy, A., Krawetz, N., Phillips, J., Shinozaki, A., Varadarajan, K., and Schulten, K. (1999) NAMD2: greater scalability for parallel molecular dynamics, *J. Comput. Phys.* 151, 283–312.
66. Brooks, B. R., Bruccoleri, R. E., Olafson, B. D., States, D. J., Swaminathan, S., and Karplus, M. (1983) CHARMM - a program for macromolecular energy, minimization, and dynamics calculations, *J. Comput. Chem.* 4, 187–217.
67. Iengar, P., Joshi, N. V., and Balaram, P. (2006) Conformational and sequence signatures in [beta] helix proteins, *Structure* 14, 529–542.
68. Pan, Y., Ma, B., Levine, A. J., and Nussinov, R. (2006) Comparison of the human and worm p53 structures suggests a way for enhancing stability, *Biochemistry* 45, 3925–3933.
69. Chen, P. (2005) Self-assembly of ionic-complementary peptides: a physicochemical viewpoint, *Colloids Surf., A* 261, 3–24.
70. Haspel, N., Zanuy, D., Ma, B., Wolfson, H., and Nussinov, R. (2004) A comparative study of amyloid fibril formation by residues 15–19 of the human calcitonin hormone: a single beta-sheet model with a small hydrophobic core, *J. Mol. Biol.* 345, 1213–1227.

BI061674A